

Studying the Pulsation of Mira Variables in the Ultraviolet

B. E. Wood¹, M. Karovska

Harvard-Smithsonian Center for Astrophysics, 60 Garden St., Cambridge, MA 02138.

`wood@head-cfa.harvard.edu, karovska@head-cfa.harvard.edu`

ABSTRACT

We present results from an empirical study of the Mg II h & k emission lines of selected Mira variable stars, using spectra from the *International Ultraviolet Explorer* (IUE). The stars all exhibit similar Mg II behavior during the course of their pulsation cycles. The Mg II flux always peaks after optical maximum near pulsation phase $\phi = 0.2 - 0.5$, although the Mg II flux can vary greatly from one cycle to the next. The lines are highly blueshifted, with the magnitude of the blueshift decreasing with phase. The widths of the Mg II lines are also phase-dependent, decreasing from about 70 km s^{-1} to 40 km s^{-1} between $\phi = 0.2$ and $\phi = 0.6$. We also study other UV emission lines apparent in the IUE spectra, most of them Fe II lines. These lines are much narrower and not nearly as blueshifted as the Mg II lines. They exhibit the same phase-dependent flux behavior as Mg II, but they do not show similar velocity or width variations.

Subject headings: stars: AGB and post-AGB — stars: variables: other — stars: oscillations — ultraviolet: stars — line: profiles

1. Introduction

At some point in their lives, many if not most stars go through an unstable phase which leads to pulsation. There are many classes of these pulsating stars. Perhaps the most famous are the Cepheid variables, which are popular mostly because of their well-defined relationship between stellar luminosity and pulsation period (typically 5–50 days) that makes these stars very useful as distance indicators.

Mira variables are another important class of stellar pulsators, having long periods of 150–500 days and luminosities that vary by as much as 6–7 magnitudes from minimum to maximum. Miras are asymptotic giant branch (AGB) stars with masses similar to that of the Sun. They have very massive, slow, cool winds, which produce a complex circumstellar environment. Observations of molecular CO lines show that Miras are often surrounded by molecular envelopes thousands of AU

¹Present address: JILA, University of Colorado, Boulder, CO 80309-0440.

in diameter. These observations yield estimates of the wind termination velocity and total mass loss rate, which are typically of order 5 km s^{-1} and $10^{-7} \text{ M}_\odot \text{ yr}^{-1}$, respectively (Young 1995). The circumstellar envelopes are rich sites for dust formation and are often found to be sources of SiO, OH, and H₂O maser emission (Diamond et al. 1994; Lopez et al. 1997).

The massive winds of Miras are believed to be driven by a combination of shocks induced by stellar pulsation, and dust formation (Bowen 1988). The shocks lift a substantial amount of material up to 1–2 stellar radii above the surface of the star. Radiation pressure on dust formed in this material then pushes it away from the star. The pulsation-induced shocks not only assist in generating the massive winds of Miras, but they also determine the atmospheric structure of these stars to a large extent. Thus, understanding the nature of the shocks and measuring their properties is essential to understanding the physics of pulsation and mass loss from pulsating stars.

The ultraviolet spectral regime is an ideal place to study radiation from the shocks. Many UV emission lines are generated from immediately behind the shocks, which are potentially very useful diagnostics for various characteristics of the shocks. Foremost among these lines are the strong Mg II h & k lines at 2800 Å.

A large number of UV spectra of Miras have been taken by the *International Ultraviolet Explorer* (IUE) over the years, and some of the basic characteristics of the Mg II h & k lines have been noted. It is known, for example, that the Mg II lines are not visible throughout part of the pulsation cycle. They typically appear at about pulsation phase $\phi = 0.1$, well after optical maximum ($\phi = 0.0$). The Mg II fluxes peak around $\phi = 0.3 – 0.45$ and then decrease until becoming undetectable at about $\phi = 0.7$ (Brugel, Willson, & Cadmus 1986; Luttermoser 1996).

For a set of LW-HI observations of S Car and R Car, Bookbinder, Brugel, & Brown (1990) showed that the Mg II h & k lines are blueshifted relative to the stellar rest frame by as much as 100 km s^{-1} , and the h line is significantly stronger than the k line. Both of these properties are very difficult to explain, as the shock speeds should be much lower than 100 km s^{-1} , and for other astronomical targets the k line is almost always found to be stronger than the h line (e.g. Robinson & Carpenter 1995).

Clearly the unusual behavior of the Mg II lines of Miras should be looked at in more detail to understand the pulsation process. In this paper, we utilize the extensive IUE data sets that exist for 5 Miras to fully characterize the behavior of the ultraviolet emission of these stars. Many pulsation cycles are sampled for each star, allowing us to see how the UV emission lines behave from one cycle to the next.

2. The IUE Archival Data

We have searched the IUE database for Miras that have been extensively observed by the satellite. In this paper, we are only interested in Miras without companion stars that may be

contaminating the UV spectrum. We are particularly interested in high resolution spectra taken with IUE’s long-wavelength cameras (i.e. LW-HI spectra). With these spectra, fully resolved profiles of detected emission lines (especially Mg II) can be analyzed. However, we also include low resolution, long-wavelength camera spectra (i.e. LW-LO spectra) in our analysis, which can at least be used to measure accurate fluxes of the Mg II lines and the background. We only consider large aperture data to ensure that our measured fluxes are accurate. Except for the Lyman- α line, which is blended with geocoronal emission, no emission lines are typically seen in Mira spectra taken with IUE’s short-wavelength SWP camera, so we are not interested in those data.

Table 1 lists the five Miras with the most extensive sets of IUE observations. (Actually, L² Pup is a semi-regular variable star rather than a Mira, but it is a long-period pulsating star similar to Miras and it has a very large IUE dataset so we include it in our analysis.) The table gives the position, distance, center-of-mass radial velocity (V_{rad}), and pulsation period of each star. The distances were taken from the Hipparcos catalog (Perryman et al. 1997).

The center-of-mass radial velocities of these stars were taken from the SIMBAD database. However, deriving true systemic center-of-mass velocities is difficult for the pulsating Miras, because different spectral features observed for these stars exhibit different velocities, and these velocities are often found to vary during the pulsation cycle. The velocities in Table 1 are based on measurements of optical absorption lines of neutral atoms, which provide plausible values for V_{rad} . Other potential measures, such as various optical emission lines, molecular radio emission lines, and maser lines, are generally blueshifted relative to the neutral atomic absorption lines by roughly 5–10 km s^{−1}. These features are probably formed either behind an outward moving shock or in the outer regions of the stellar atmosphere where the massive wind of the star is being accelerated (Joy 1954; Merrill 1960; Wallerstein 1975; Gillet 1988). Note that infrared CO emission lines, which can also be used to estimate stellar center-of-mass radial velocities, generally suggest velocities that are blueshifted relative to the optical velocities by ~ 5 km s^{−1} (Hinkle 1978; Hinkle & Barnbaum 1996; Hinkle, Lebzelter, & Scharlach 1997).

In order to determine how UV emission varies during the pulsation cycle it is necessary to derive accurate pulsation phases, which requires knowledge of the pulsation period and a zero-phase date. All of the Miras in Table 1 have been monitored for many decades, and their average periods are well known. However, the periods of Miras can sometimes differ from this average. Therefore, in order to derive the most accurate phases, we sought to determine the average period and zero-phase of our Miras during IUE’s lifetime only (1978–1996).

The American Association of Variable Star Observers (AAVSO) has a long-term program to monitor hundreds of Miras using observations from amateur astronomers around the world (Mattei & Foster 1997). Using AAVSO data obtained from the World Wide Web, we derived the pulsation periods listed in Table 1. The derived periods of S Car, R Car, and R Leo are within a day of the accepted long-term average values (see, e.g., Hirshfeld & Sinnott 1985), but the derived period of L² Pup is 4 days shorter and that of T Cep is 11 days longer. For these two stars, the accuracy

of the computed pulsation phases is improved significantly with the use of the derived periods in Table 1. As mentioned above, L² Pup is a semi-regular variable rather than a traditional Mira, but it is similar to Miras in other respects so it is included in our sample. Because of the irregularity of its period, the accuracy of the pulsation phases we derive is limited to about ± 0.2 . The pulsation of the other stars on our list is far more regular, and we estimate that the phases we use for these stars are accurate to within about ± 0.05 .

Table 1 lists the number of LW-HI and LW-LO spectra available for each star. In each case, the available data provide reasonably good coverage of at least 2–3 different pulsation cycles. The data were extracted from the IUE Final Archive. The spectra in the archive were processed using the NEWSIPS software, which became available near the end of the IUE’s 18-year lifetime in the mid-1990s. This software corrects the fixed pattern noise problem that plagued spectra processed with the older IUESIPS software, and improves signal-to-noise by up to a factor of 2 for high resolution spectra. The NEWSIPS software is described in detail by Nichols & Linsky (1996).

3. Data Analysis

3.1. The LW-LO Spectra

Figure 1 illustrates the behavior of the near UV spectrum of the Mira R Car during a typical pulsation cycle in 1986–1987. The primary spectral feature visible in the LW-LO spectra is the Mg II h & k feature at 2800 Å, which appears shortly after optical maximum, achieves a maximum flux around $\phi = 0.4 – 0.5$, and then declines. The Fe II UV1 multiplet lines at 2620 Å are also visible when Mg II is at its brightest.

We developed a semi-automated routine to measure the Mg II fluxes from the LW-LO spectra of our stars. For each spectrum, the underlying background flux is estimated using the flux in the surrounding spectral region. The reasonableness of this computed background is verified visually. After subtracting the background from the spectrum, the Mg II flux is then computed by direct integration. The error vector provided by the NEWSIPS software then allows us to estimate the 1σ uncertainty for this flux. Three spectra from R Leo show substantial background emission at an unexpected phase, which we believe indicates contamination by scattered solar light, so these spectra are not used.

In Figure 2, we plot the Mg II fluxes as a function of pulsation phase for all the stars in our sample. We use thick symbols to indicate Mg II lines with 3 or more pixels that have been flagged by NEWSIPS as being potentially inaccurate, usually due to overexposure. These fluxes should be considered more uncertain than the plotted 1σ error bars would suggest. In general, however, these fluxes are not wildly discrepant from fluxes of better exposed lines measured closely in time. Dashed lines connect points that are within the same pulsation cycle, excluding cases where the points are separated by over 0.4 phase.

Figure 2 shows that the pulsation cycles of each star are all consistent with the general rule of a flux maximum around $\phi = 0.2 - 0.5$. However, there are substantial flux differences from one cycle to the next. The R Car data set shows the most extreme such variability, with the Mg II fluxes reaching only about 1×10^{-13} ergs cm $^{-2}$ s $^{-1}$ in one cycle and approaching 1×10^{-10} ergs cm $^{-2}$ s $^{-1}$ during another. In contrast, the Mg II fluxes of S Car differ by less than an order of magnitude from one cycle to the next, this despite the fact that S Car has one of the largest IUE LW-LO databases. The other relatively short period pulsator in our sample, L² Pup, seems to behave similarly. The data points show more scatter for L² Pup, but this is probably due to inaccuracies in the estimated pulsation phases caused by the irregular period of this star (see §2). A comparison of L² Pup’s Mg II and optical variability has been presented by Brugel, Willson, & Bowen (1990).

The phase of maximum Mg II flux differs somewhat for the five stars, with S Car appearing to have the earliest maximum and R Leo the latest. One of the brighter Mg II cycles of R Leo is particularly interesting for showing substantial Mg II flux very near optical maximum at $\phi = 0.04$ (observations LWP21679 and LWP21680). We generally do not detect significant Mg II flux this close to $\phi = 0.0$ for any of our stars (excluding L² Pup because of its uncertain phases), but apparently there can be exceptions to this rule. By inspecting the AAVSO light curve we confirmed that the strong Mg II lines had in fact been observed very near optical maximum.

3.2. The LW-HI Spectra

3.2.1. The Mg II h & k Lines

Turning our attention to the LW-HI spectra, in Figures 3–7 we display the observed Mg II h & k line profiles for the five stars in our sample. The k line is shown as a solid line and the h line is represented by a dotted line. The spectra are shown on a velocity scale in the stellar rest frame, assuming the stellar center-of-mass velocities listed in Table 1, and assuming rest wavelengths in air of 2802.705 Å and 2795.528 Å for the h and k lines, respectively. The date, time, and pulsation phase of each observation are indicated in the figures. Cosmic ray hits, which are apparent in the original spectra as very narrow, bright spectral features not observed in other spectra, have been identified and removed manually. One S Car spectrum with wildly discrepant properties (LWP12197) was removed from the analysis and is therefore not shown in Figure 5.

Many of the S Car spectra were taken with the star deliberately offset within IUE’s large aperture. This results in an inaccurate wavelength calibration. Fortunately, there is a set of nine observations taken on 1991 March 9–13 with different offsets (see Fig. 5). After measuring the centroids of the Mg II h line (see below), we were able to see from these data how the offsets affected the h line centroid and we used this information to correct the wavelengths of all the S Car spectra obtained with aperture offsets. The spectra in Figure 5 are the corrected spectra.

In almost every spectrum in Figures 3–7, the k line is contaminated by substantial absorption

centered at a stellar rest frame velocity of about -70 km s^{-1} . This absorption is due to lines of Fe I and Mn I with rest wavelengths in air of 2795.005 Å and 2794.816 Å, respectively (Luttermoser et al. 1989; Luttermoser & Mahar 1998). Because the mutilation of the k line by these overlying neutral absorbers is generally severe, we focus most of our attention on the more pristine h line.

Another concern is interstellar absorption, which should affect both the h and k lines at the same velocity. The one star whose spectrum we know will *not* be affected by the ISM is S Car, because its extremely large $+289 \text{ km s}^{-1}$ center-of-mass velocity will shift the Mg II lines well away from any ISM absorption. The h line of L² Pup shows absorption at about -40 km s^{-1} (see Fig. 7). The ISM velocity predicted for this line of sight by the local ISM flow vector of Lallement et al. (1995) is -43 km s^{-1} after shifting to the stellar rest frame. Thus, it seems likely that this is indeed interstellar absorption, although for lines of sight as long as those towards the stars in our sample, ISM components could potentially be present with significantly different velocities than that predicted by the local flow vector.

The h lines of R Leo, R Car, and T Cep do not appear to be contaminated by any obvious ISM absorption features. For R Leo and T Cep, the ISM velocities predicted by the local flow vector (-4 and $+14 \text{ km s}^{-1}$, respectively) suggest that the ISM absorption may lie outside of the observed Mg II emission (see Figs. 3 and 6). For the R Car line of sight, the local flow vector predicts ISM absorption at -30 km s^{-1} , which falls just within the red side of the h line. No obvious absorption is seen, however, suggesting that the ISM column density for this particular line of sight may be quite low. This is not necessarily unusual, as other lines of sight with distances of $\gtrsim 100 \text{ pc}$ have been found to have very low H I column densities of $\sim 10^{18} \text{ cm}^{-2}$ (Gry et al. 1995; Piskunov et al. 1997).

We will assume that the Mg II h line profiles of R Leo, R Car, and T Cep are at most only mildly affected by ISM absorption, meaning that for these three stars and S Car we can be reasonably confident that any substantial line profile differences we might find are due to intrinsic differences in the stellar spectra. The Mg II h line profiles of these four stars often appear to be slightly asymmetric, with a red side that is steeper than the blue side. Nevertheless, the profiles can be represented reasonably well as a Gaussian, and can therefore be quantified with Gaussian fits. We developed a semi-automated procedure to fit all Mg II h lines detected with enough signal-to-noise (S/N) for a meaningful fit to be performed. The quality of all fits was verified visually. For spectra without strong Mg II h lines, we estimated a line flux by direct integration as we did for the LW-LO spectra. For L² Pup, we measured h line fluxes for *all* the spectra in this manner, since we could not accurately fit Gaussians to the ISM-contaminated line profiles observed for this star.

In Figures 8–10, we plot versus pulsation phase the Mg II h line fluxes, centroid velocities, and widths measured from the LW-HI spectra of the stars in our sample. As in Figure 2, dotted lines connect points within the same pulsation cycle, and thick data points indicate h lines with three or more pixels flagged as being overexposed. The 1σ uncertainties shown in the figure were estimated using the procedures outlined by Lenz & Ayres (1992). The flux variations seen in Figure 8 are

essentially the same as those seen in the LW-LO data (see Fig. 2). Note once again how much the Mg II fluxes vary from one cycle to the next for R Car.

Bookbinder et al. (1990) found that the Mg II lines in selected observations of S Car and R Car were substantially blueshifted. Figure 9 demonstrates that this behavior is common to all the Mg II lines observed by IUE for all the Miras in our sample. Furthermore, Figure 9 also reveals a strong correlation between line velocity and pulsation phase, in which the magnitude of the line blueshifts decreases with pulsation phase. For example, between $\phi = 0.2$ and $\phi = 0.6$ the line velocities of S Car change from about -100 km s^{-1} to -50 km s^{-1} , and those of T Cep change from -50 km s^{-1} to -30 km s^{-1} . Note that even though we are using Gaussians to fit the Mg II profiles, this does *not* imply that Mg II h & k are optically thin or that the large blueshifts of these lines actually represent gas velocities (see §3.2.2).

This velocity behavior exactly mimics the behavior of the optical Ca II H & K lines of Miras, which also have blueshifted velocities that typically change from about -100 km s^{-1} to -40 km s^{-1} between $\phi = 0.2$ and $\phi = 0.6$ (Merrill 1952; Buscombe & Merrill 1952). Thus, opacity effects and atmospheric flow fields appear to induce the same line behavior in both the Mg II and Ca II lines. Furthermore, many Cepheid variables appear to exhibit similar behavior, suggesting that these phase-dependent velocity variations may be typical for stellar pulsators in general (Merrill 1960).

The data in Figure 9 suggest a possible correlation between pulsation period and line velocity, with the shortest period Mira in our sample (S Car) having the largest blueshifts, and the longest period star (T Cep) having the smallest. The R Car data suggest another possible correlation. For the pulsation cycle with the largest Mg II fluxes, the Mg II h lines of R Car are more blueshifted than they are during the weaker cycles. Unfortunately, our sample of stars and the number of well-sampled pulsation cycles per star is very small, making it difficult to truly establish these correlations.

Figure 10 demonstrates that a well-defined phase dependence also exists for the line widths, which are quantified in Figure 10 as full-widths-at-half-maxima (FWHM). The line width behavior is very similar for all the stars, with a decrease from about 70 km s^{-1} to 40 km s^{-1} between $\phi = 0.2$ and $\phi = 0.6$.

3.2.2. Other Lines in the IUE LW-HI Spectra

The Mg II h & k lines are by far the brightest lines that appear in the LW-HI spectra of Miras, but they are not the only lines present. During pulsation cycles that produce strong Mg II lines, other lines also appear out of the background noise of the LW-HI spectra.

The largest Mg II fluxes observed for any star in our sample were observed during the 1989–90 pulsation cycle of R Car, during which Mg II h line fluxes reached up to $5 \times 10^{-11} \text{ ergs cm}^{-2} \text{ s}^{-1}$ (see Figs. 4 and 8). Figure 11 shows three sections of an LW-HI spectrum taken during this period.

These sections contain all of the obvious real emission features apparent in the full spectrum. The expected line locations of several multiplets are indicated in the figure, which accounts for most of the observed emission features. The spectrum is dominated by several multiplets of Fe II lines (UV1, UV32, UV60, UV62, and UV63). The Mg II h & k (UV1) lines are of course apparent, as perhaps are two much weaker Mg II lines of the UV3 multiplet. The intersystem Al II] (UV1) line at 2669.155 Å is easily visible. Luttermoser & Mahar (1998) observed the feature at 2823 Å in an HST/GHRS spectrum of the Mira R Hya, and identified it as an Fe I (UV44) 2823.276 Å line which is fluoresced by the Mg II k line. A couple other emission features in Figure 11 can also be identified with Fe I (UV44) lines.

The lines seen in Figure 11 have previously been observed in many IUE and HST/GHRS spectra of red giant stars (Judge & Jordan 1991; Carpenter, Robinson, & Judge 1995; Robinson, Carpenter, & Brown 1998). The Al II] line and most of the Fe II lines are formed by collisional excitation, as are the Mg II h & k lines, but Judge, Jordan, & Feldman (1992) find that the UV62 and UV63 multiplet lines of Fe II are excited by a combination of collisional excitation and photoexcitation by photospheric emission at optical wavelengths.

The flux behavior of all the lines in Figure 11 parallels that of Mg II, increasing to a maximum near $\phi = 0.3 - 0.4$ and then decreasing. Thus, the Fe II and Al II] lines presumably originate in atmospheric locations similar to Mg II h & k. Note that many of the lines apparent in Figure 11 were only observed during this one particularly bright cycle of R Car, presumably being too weak to be detected during weaker cycles on R Car and the other stars. For a selection of the brightest emission lines, we used an automated fitting procedure like that described in §3.2.1 to fit Gaussians to the lines of all the stars in our sample, whenever the lines are clearly detected. The lines measured in this manner are listed in Table 2. For L² Pup, no observed cycle was bright enough to detect any of these lines, and for S Car only the brightest Fe II line at 2625.667 Å could ever be clearly detected.

For the observations in which the lines are observed, we find that line flux ratios among the various Fe II lines are always similar to those seen in Figure 11, as are Mg II/Fe II flux ratios. For example, the (Mg II $\lambda 2803$)/(Fe II $\lambda 2626$) ratio is always about 20. The Fe II and Mg II/Fe II flux ratios found for the Miras are somewhat different from those observed in red giants, but not radically so.

However, the Fe II line *profiles* are very different. For normal red giant stars, most of the Fe II lines are clearly opacity broadened and have profiles very different from that of a simple Gaussian (Judge & Jordan 1991; Carpenter et al. 1995). In contrast, the Fe II lines of Miras are very narrow, Gaussian-shaped emission features, with widths at or near the IUE's instrumental resolution of ~ 0.2 Å. This is why we could accurately fit the lines with single Gaussians. The exception is the broader Fe II 2599.394 Å line, which should have the highest opacity of all the Fe II lines.

The widths and velocities of the lines listed in Table 2 do not appear to exhibit any substantial phase dependent behavior, in contrast to Mg II h & k. As an example, in Figure 12 we plot the

velocities of the Fe II 2625.667 Å line as a function of pulsation phase for the four Miras in which this line was occasionally detected. Only S Car has a hint of phase dependence, with some evidence for a small increase in velocity with phase. Much of the scatter seen in Figure 12 could be due to uncertainties in target centering, which can induce systematic velocity errors of $\pm 5 \text{ km s}^{-1}$ (Wood & Ayres 1995).

Since there is little if any phase dependence in the velocities of the lines listed in Table 2, we compute a weighted average and standard deviation for all the measurements of all the lines (Bevington & Robinson 1992), and in Table 2 these velocities are listed for each Mira in our sample. For R Leo, R Car, and S Car, all of the lines are blueshifted $5 - 15 \text{ km s}^{-1}$. The Fe II 2599.394 Å line is once again an exception, showing significantly larger blueshifts.

The lines of T Cep behave differently, as they do not show systematic blueshifts relative to the star. The Mg II lines of T Cep are also not as blueshifted as the other stars (see §3.2.1 and Fig. 9). It is difficult to identify a reason for this difference in behavior, but perhaps the center-of-mass velocity we are assuming for this star is off by $\sim 10 \text{ km s}^{-1}$. The difficulties in defining center-of-mass velocities for Miras have already been discussed in §2.

The large blueshifts observed for the Mg II lines are unlikely to be direct measurements of outflow velocities. The shock velocities present in Miras are expected to be of order $10 - 20 \text{ km s}^{-1}$, although this issue is still a matter of debate (Bowen 1988; Gillet 1988; Hinkle et al. 1997). Thus, the $5 - 15 \text{ km s}^{-1}$ blueshifts seen for most of the Fe II and Al II] lines of R Leo, R Car, and S Car are more likely to be measuring the true outflow velocities of shocked material. The larger widths and blueshifts of the Mg II lines are probably due to opacity effects, similar to the findings of Judge et al. (1993) for non-Mira M-type giants. The similar behavior of the Fe II $\lambda 2599$ line suggests that this line is influenced by similar opacity effects, which is reasonable since this line should have the highest opacity of any of the Fe II lines.

The other Fe II lines will have substantially lower optical depths than Mg II h & k and Fe II $\lambda 2599$, and some may even be optically thin. The Al II] $\lambda 2669$ line should also have very low opacity, since it is a semi-forbidden transition. Thus, the Fe II and Al II] line centroids should be more indicative of the true outflow velocities of the shocked material, and the line widths (which are actually unresolved) should be more indicative of turbulent velocities within the shocked material.

Interpreting the difference between the behavior of the Mg II lines and that of the less opaque lines could be very important for understanding the structure of the shocks propagating through Mira atmospheres. In future work, we hope to explore possible reasons why the Mg II lines are broader and more blueshifted than the less optically thick lines.

4. Summary

We have compiled IUE observations of 5 Mira variables with substantial IUE data sets in order to study the properties of emission lines seen in the UV spectra of these stars, which are believed to be formed behind outwardly propagating shocks in the atmospheres of these pulsating stars. Our findings are summarized as follows:

1. We confirm the phase-dependent Mg II flux behavior previously reported for Mira variables (e.g. Brugel et al. 1986), which is observed for all the pulsation cycles that we study: the Mg II flux rises after optical maximum, peaks near $\phi = 0.2 - 0.5$, and then decreases. For some Miras (e.g. R Car) the amount of Mg II flux produced during a pulsation cycle can vary by 2–3 orders of magnitude from one cycle to the next, while for others (e.g. S Car) the flux behavior is more consistent.
2. The Mg II k lines are almost always contaminated with circumstellar absorption lines of Fe I and Mn I, making analysis of the line profile very difficult.
3. The Mg II h line is always blueshifted, with the magnitude of the blueshift decreasing with pulsation phase. The blueshifts vary somewhat from star to star and cycle to cycle, but typical velocity changes are from -70 km s^{-1} to -40 km s^{-1} from $\phi = 0.2$ to $\phi = 0.6$. Note, however, that these line shifts do not represent the actual gas velocities at the formation depths of these lines, because of the high opacity of Mg II h & k. These velocity variations are very similar to those of the optical Ca II H & K lines.
4. The width of the Mg II h line decreases from about 70 km s^{-1} to 40 km s^{-1} between $\phi = 0.2$ and $\phi = 0.6$.
5. In addition to the Mg II lines, other lines of Fe II, Fe I, and Al II] are also observed in IUE LW-HI spectra. The fluxes of these lines show the same phase-dependent behavior as the Mg II lines.
6. Unlike Mg II, these other emission lines tend to be very narrow and do not show phase-dependent velocity and width variations. Except for Fe II $\lambda 2599$, the Fe II and Al II] lines of most of the Miras show blueshifts of $5 - 15 \text{ km s}^{-1}$, which may indicate the flow velocity of the shocked material. In contrast, the lines of T Cep do not show any significant line shifts, although we speculate that perhaps this is due to an uncertain center-of-mass velocity for this star.

We would like to thank the referee, Dr. D. Luttermoser, for many useful comments on the manuscript. MK is a member of the Chandra X-ray Center, which is operated under contract NAS-839073, and is partially supported by NASA. In this research, we have used, and acknowledge with thanks, data from the AAVSO International Database, based on observations submitted to the AAVSO by variable star observers worldwide.

REFERENCES

- Bevington, P. R., & Robinson, D. K. 1992, Data Reduction and Error Analysis for the Physical Sciences (New York: McGraw-Hill)
- Bookbinder, J. A., Brugel, E. W., & Brown, A. 1989, *ApJ*, 342, 516
- Bowen, G. H. 1988, *ApJ*, 329, 299
- Brugel, E. W., Willson, L. A., & Bowen, G. 1990, in Evolution in Astrophysics: IUE Astronomy in the Era of New Space Missions, (Noordwijk: ESA SP-310), 241
- Brugel, E. W., Willson, L. A., & Cadmus, R. 1986, in New Insights in Astrophysics: Eight Years of UV Astronomy with IUE, (Noordwijk: ESA SP-263), 213
- Buscombe, W., & Merrill, P. W. 1952, *ApJ*, 116, 525
- Carpenter, K. G., Robinson, R. D., & Judge, P. G. 1995, *ApJ*, 444, 424
- Diamond, P. J., Kemball, A. J., Junor, W., Zensus, A., Benson, J., & Dhawan, V. 1994, *ApJ*, 430, L61
- Gillet, D. 1988, *A&A*, 190, 200
- Gry, C., Lemonon, L., Vidal-Madjar, A., Lemoine, M., & Ferlet, R. 1995, *A&A*, 302, 497
- Hinkle, K. H. 1978, *ApJ*, 220, 210
- Hinkle, K. H., & Barnbaum, C. 1996, *AJ*, 111, 913
- Hinkle, K. H., Lebzelter, T., & Scharlach, W. W. G. 1997, *AJ*, 114, 2686
- Hirshfeld, A., & Sinnott, R. W. 1985, Sky Catalogue 2000.0, Vol. 2 (Cambridge: Sky Publishing Corporation)
- Joy, A. H. 1954, *ApJS*, 1, 39
- Judge, P. G., & Jordan, C. 1991, *ApJS*, 77, 75
- Judge, P. G., Jordan, C., & Feldman, U. 1992, *ApJ*, 384, 613
- Judge, P. G., Luttermoser, D. G., Neff, D. H., Cuntz, M., & Stencel, R. E. 1993, *AJ*, 105, 1973
- Lallement, R. L., Ferlet, R., Lagrange, A. M., Lemoine, M., & Vidal-Madjar, A. 1995, *A&A*, 304, 461
- Lenz, D. D., & Ayres, T. R. 1992, *PASP*, 104, 1104
- Lopez, B., et al. 1997, *ApJ*, 488, 807

- Luttermoser, D. G. 1996, in Cool Stars, Stellar Systems, and the Sun, Ninth Workshop, ed. R. Pallavicini & A. K. Dupree (San Francisco: ASP Conf. Ser., Vol. 109), 535
- Luttermoser, D. G., Johnson, H. R., Avrett, E. H., & Loeser, R. 1989, *ApJ*, 345, 543
- Luttermoser, D. G., & Mahar, S. 1998, in Cool Stars, Stellar Systems, and the Sun, Tenth Workshop, ed. R. A. Donahue & J. A. Bookbinder (San Francisco: ASP Conf. Ser., Vol. 154), 1613
- Mattei, J. A., & Foster, G. 1997, *BAAS*, 29, 1284
- Merrill, P. W. 1952, *ApJ*, 116, 337
- Merrill, P. W. 1960, in *Stellar Atmospheres*, ed. J. L. Greenstein (Chicago: The Univ. of Chicago Press), 509
- Nichols, J. S., & Linsky, J. L. 1996, *PASP*, 111, 517
- Perryman, M. A. C., et al. 1997, *A&A*, 323, L49
- Piskunov, N., Wood, B. E., Linsky, J. L., Dempsey, R. C., & Ayres, T. R. 1997, *ApJ*, 474, 315
- Robinson, R. D., & Carpenter, K. G. 1995, *ApJ*, 442, 328
- Robinson, R. D., Carpenter, K. G., & Brown, A. 1998, *ApJ*, 503, 396
- Wallerstein, G. W. 1975, *ApJS*, 29, 375
- Wood, B. E., & Ayres, T. R. 1995, *ApJ*, 443, 329
- Young, K. 1995, *ApJ*, 445, 872

Table 1. Mira Variables with Large IUE Data Sets

| Star | RA (J2000) | DEC (J2000) | Distance (pc) | V_{rad} (km s $^{-1}$) | Period (days) | # of IUE Spectra | |
|--------------------|---------------|----------------|------------------|------------------------------|------------------|------------------|---------|
| | | | | | | (LW-HI) | (LW-LO) |
| S Car | 10:09:22 | –61°32'57" | 405 ± 103 | +289 | 150 | 42 | 67 |
| R Car | 9:32:15 | –62°47'20" | 128 ± 14 | +28 | 308 | 28 | 45 |
| L ² Pup | 7:13:32 | –44°38'39" | 61 ± 5 | +53 | 136 | 15 | 68 |
| T Cep | 21:09:32 | 68°29'27" | 210 ± 33 | –12 | 399 | 15 | 32 |
| R Leo | 9:47:33 | 11°25'44" | 101 ± 21 | +13 | 313 | 13 | 58 |

Table 2. Line Velocities

| Ion | Wavelength | Multiplet | Velocity (km s ⁻¹) | | | |
|--------|------------|-----------|--------------------------------|-----------------|-----------------|-----------------|
| | | | R Leo | R Car | S Car | T Cep |
| Al II] | 2669.155 | 1 | -7.1 ± 8.7 | -4.7 ± 3.3 | ... | 1.5 ± 4.7 |
| Fe I | 2823.276 | 44 | -5.6 ± 9.6 | -3.9 ± 5.0 | ... | 3.2 ± 4.0 |
| Fe II | 2598.368 | 1 | -14.5 ± 9.1 | -10.7 ± 1.4 | ... | 3.8 ± 8.7 |
| Fe II | 2599.394 | 1 | -24.8 ± 4.8 | -36.1 ± 2.6 | ... | -16.3 ± 5.2 |
| Fe II | 2607.085 | 1 | -14.4 ± 5.9 | -10.0 ± 2.8 | ... | ... |
| Fe II | 2611.873 | 1 | -12.9 ± 2.5 | -8.5 ± 2.1 | ... | -3.8 ± 10.0 |
| Fe II | 2617.616 | 1 | -15.9 ± 6.1 | -9.6 ± 2.8 | ... | -11.5 ± 3.3 |
| Fe II | 2620.408 | 1 | -9.5 ± 8.4 | -5.9 ± 2.7 | ... | 4.8 ± 2.6 |
| Fe II | 2625.667 | 1 | -12.8 ± 6.0 | -10.7 ± 2.7 | -15.9 ± 4.9 | -2.7 ± 1.8 |
| Fe II | 2628.292 | 1 | -15.6 ± 6.5 | -9.2 ± 2.5 | ... | -3.7 ± 3.4 |
| Fe II | 2732.440 | 32 | -13.2 ± 4.8 | -3.5 ± 1.8 | ... | 3.0 ± 3.7 |
| Fe II | 2759.334 | 32 | -9.1 ± 4.3 | -5.6 ± 1.9 | ... | 3.2 ± 3.6 |
| Fe II | 2926.587 | 60 | -12.7 ± 6.8 | -8.2 ± 4.4 | ... | 1.5 ± 4.2 |
| Fe II | 2953.773 | 60 | -9.0 ± 3.5 | -4.1 ± 3.8 | ... | -2.0 ± 4.8 |
| Fe II | 2730.734 | 62 | -18.2 ± 10.4 | -6.9 ± 3.8 | ... | ... |
| Fe II | 2743.197 | 62 | -5.2 ± 6.4 | -4.6 ± 3.4 | ... | 6.2 ± 4.1 |
| Fe II | 2755.735 | 62 | -9.3 ± 6.3 | -8.1 ± 2.6 | ... | 0.6 ± 4.2 |
| Fe II | 2727.538 | 63 | -18.6 ± 9.6 | -14.3 ± 4.7 | ... | ... |
| Fe II | 2739.547 | 63 | -12.8 ± 8.3 | -7.2 ± 3.4 | ... | 5.2 ± 2.7 |

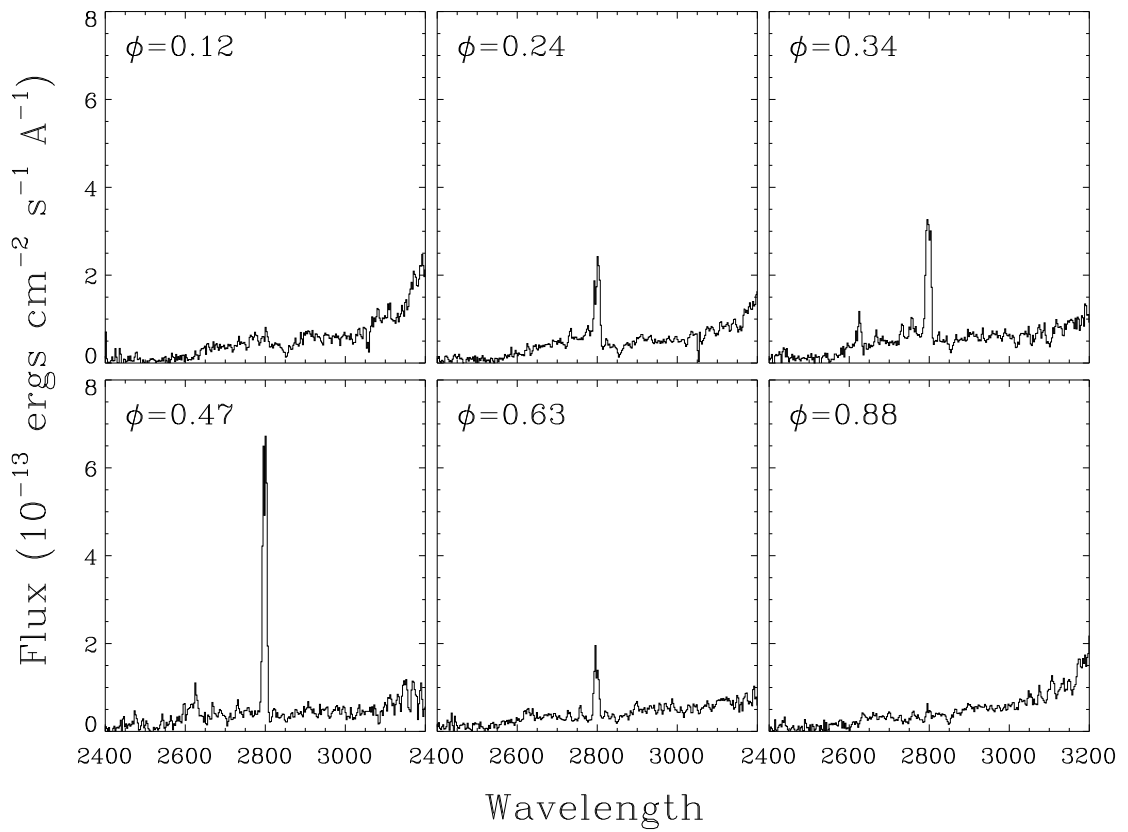


Fig. 1.— Six low resolution IUE spectra of R Car, illustrating the variation in Mg II h & k line flux as a function of pulsation phase for one pulsation cycle.

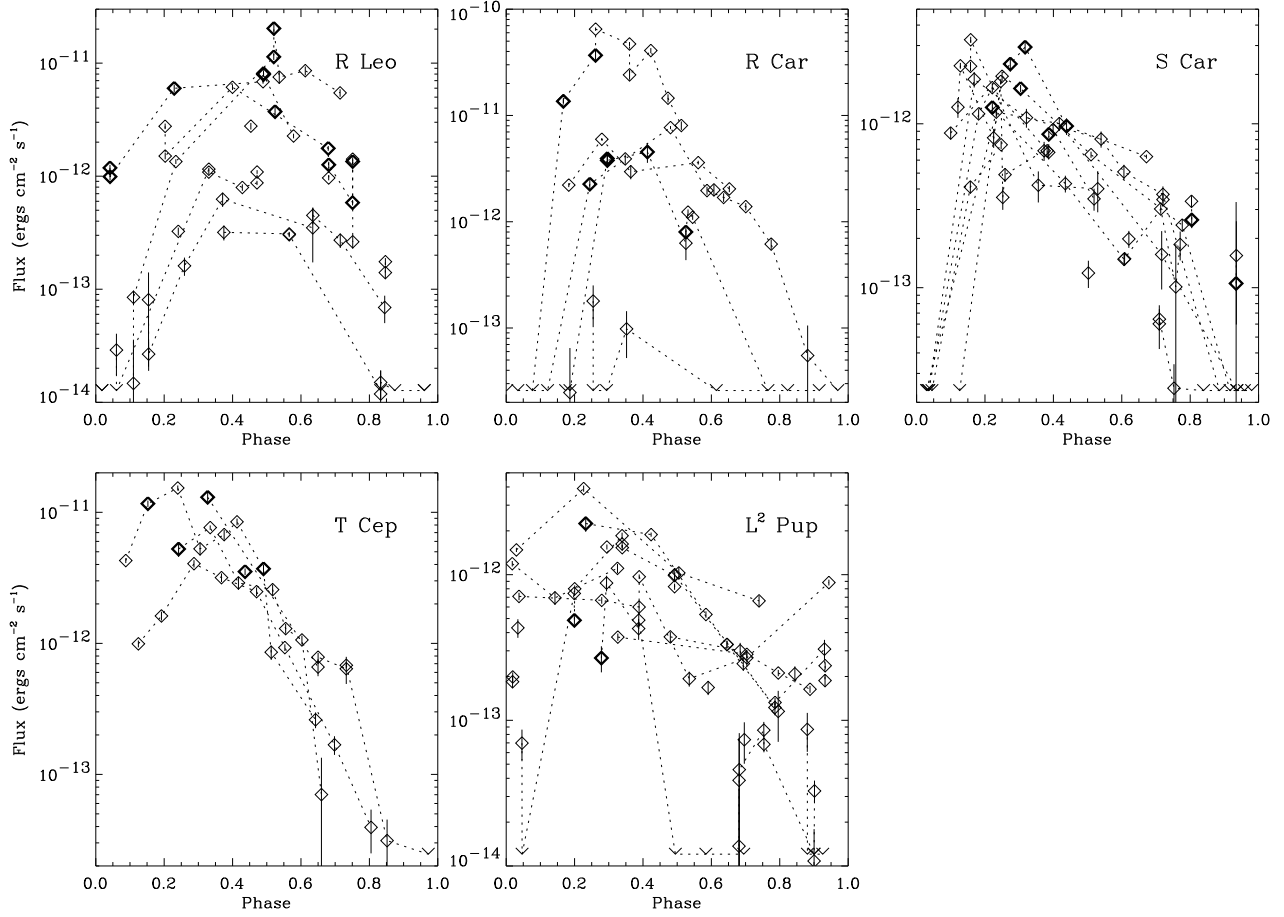


Fig. 2.— The Mg II line fluxes measured from IUE LW-LO spectra, plotted versus pulsation phase. Dotted lines connect points within the same pulsation cycle. Thick symbols identify potentially inaccurate data points (usually due to overexposure), as indicated by NEWSIPS data quality flags.

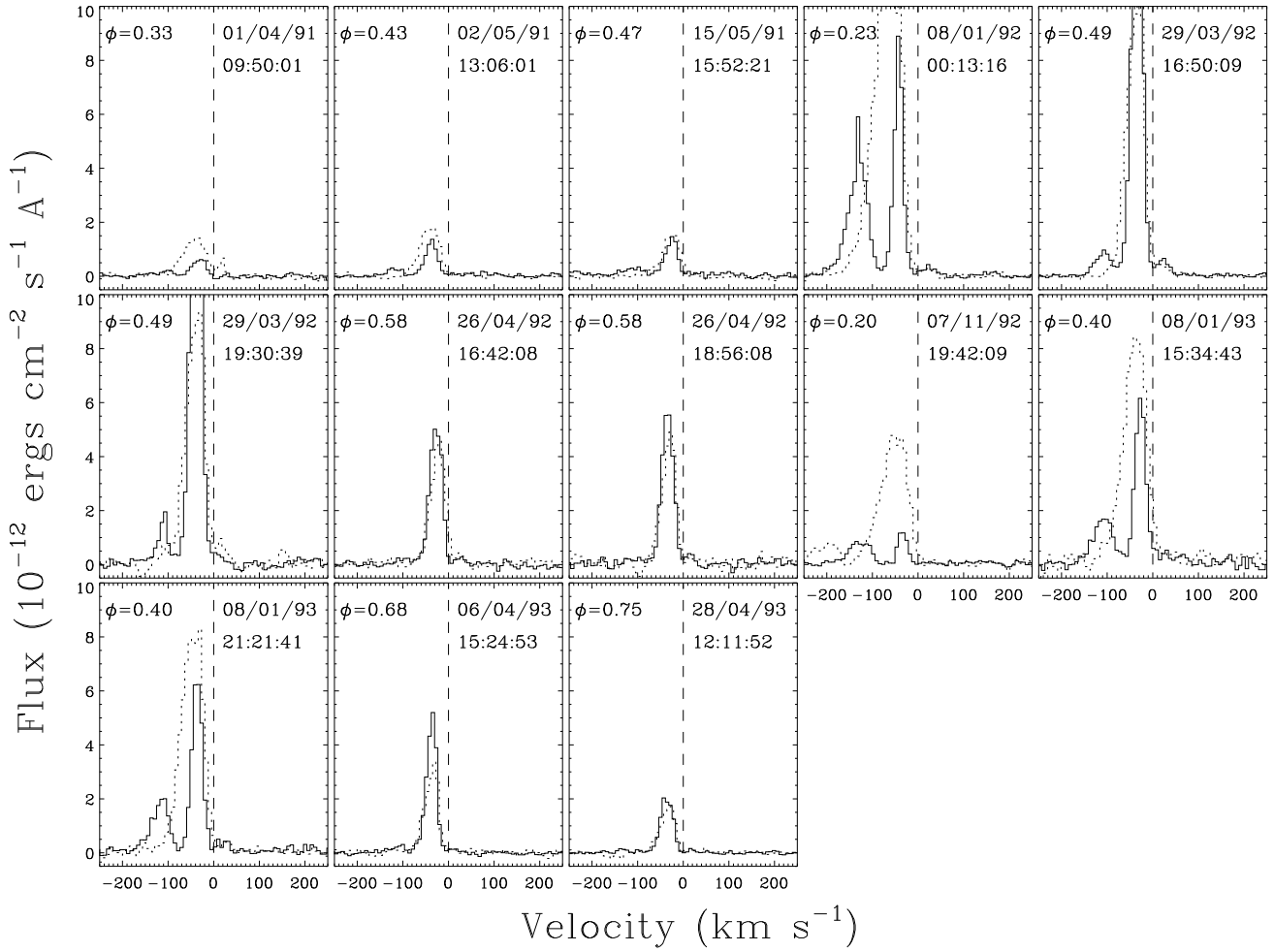


Fig. 3.— The IUE LW-HI observations of the Mg II h (dotted lines) and k (solid lines) line profiles of R Leo. The pulsation phase, date, and UT time of observation are indicated in each panel. The spectra are plotted on a velocity scale in the stellar rest frame.

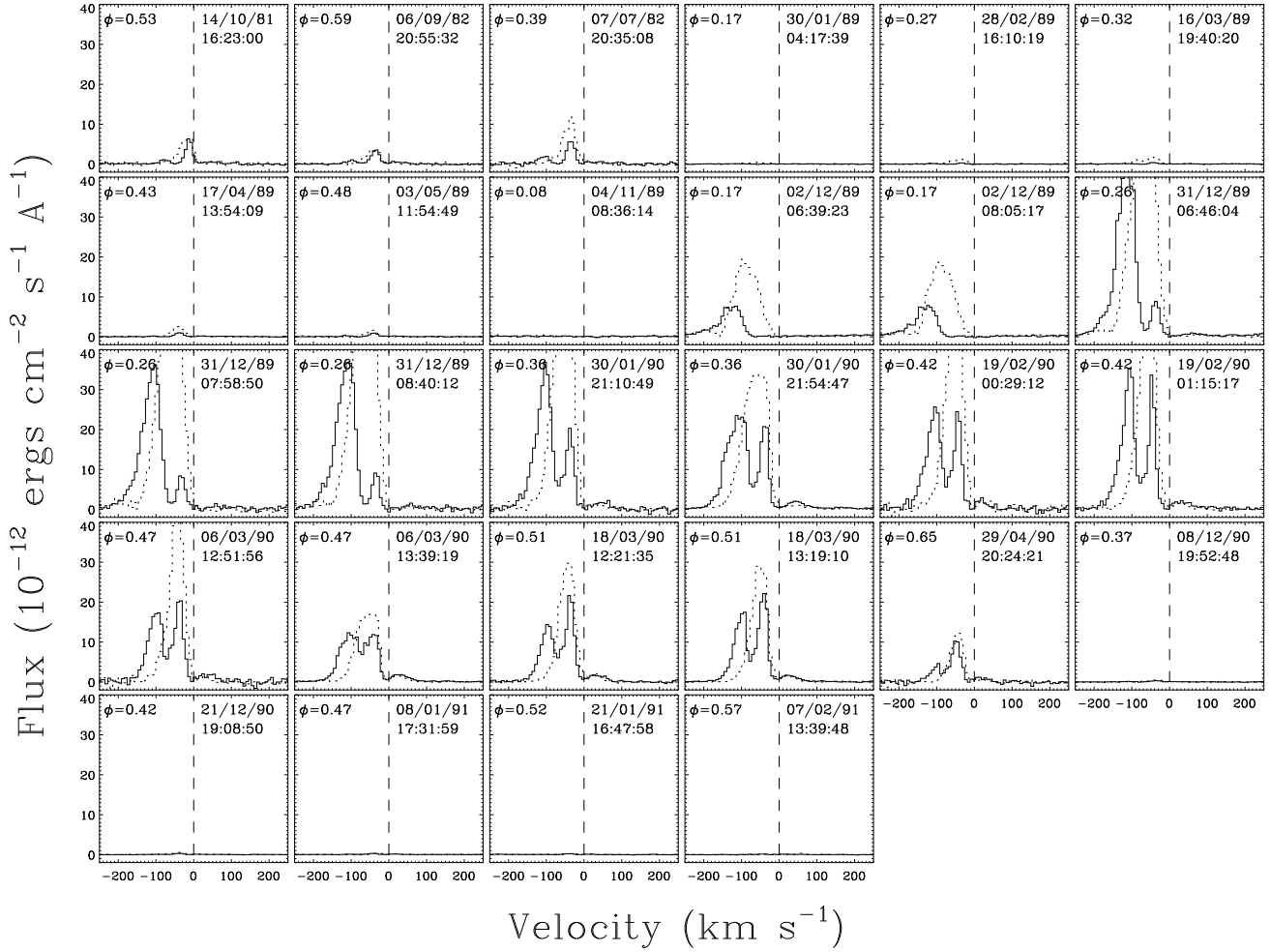


Fig. 4.— Same as Fig. 3, for R Car.

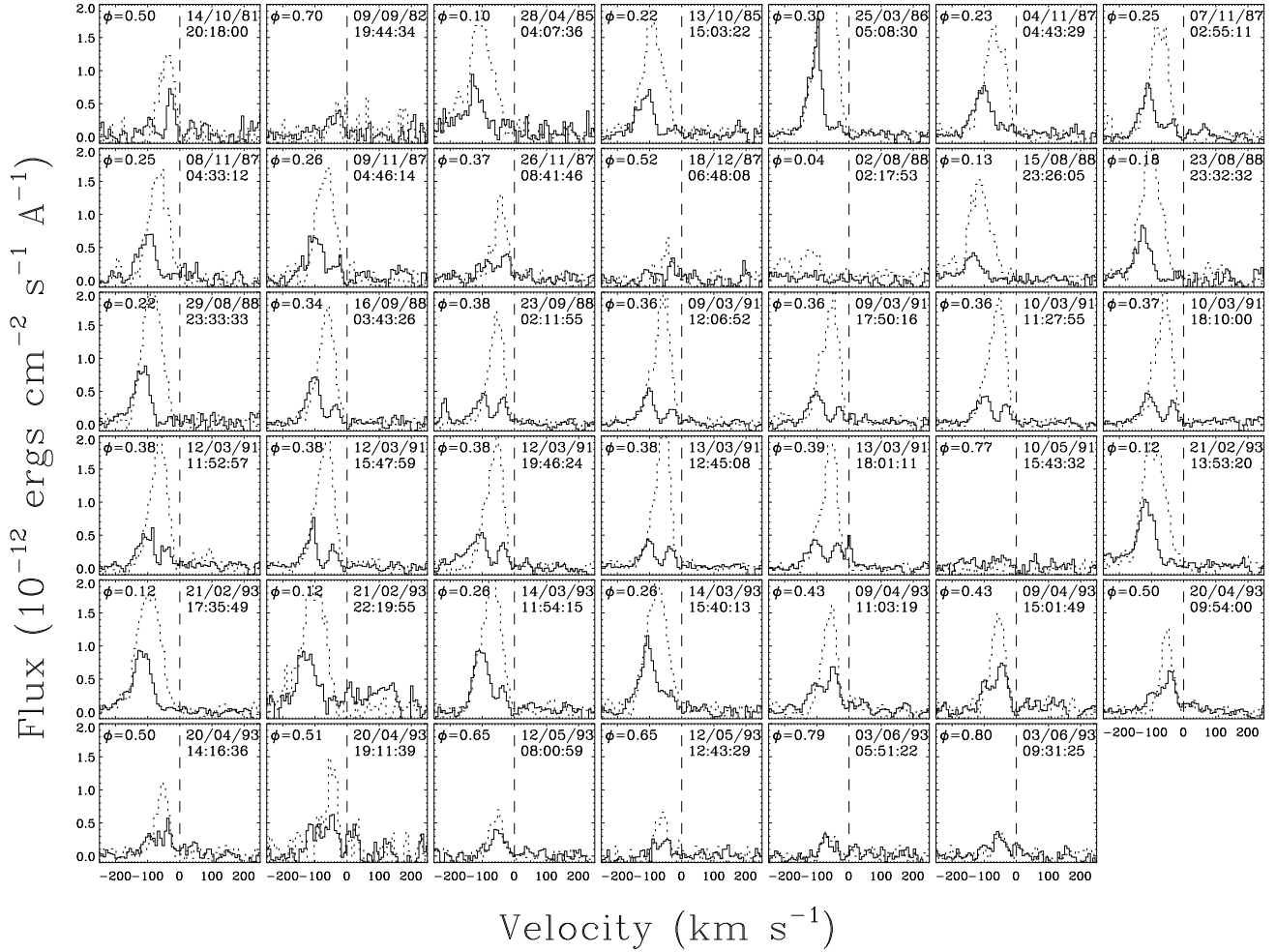


Fig. 5.— Same as Fig. 3, for S Car.

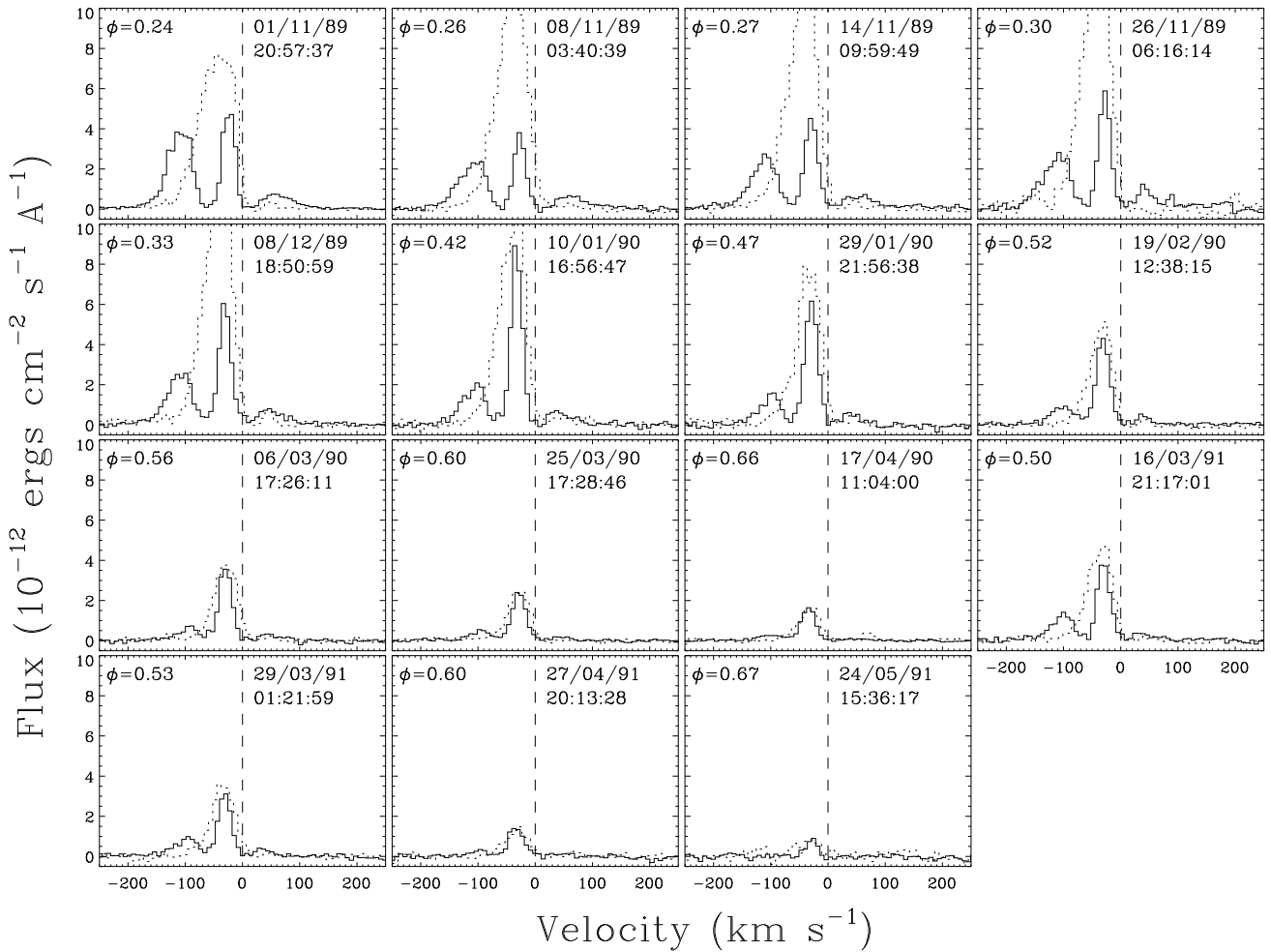


Fig. 6.— Same as Fig. 3, for T Cep.

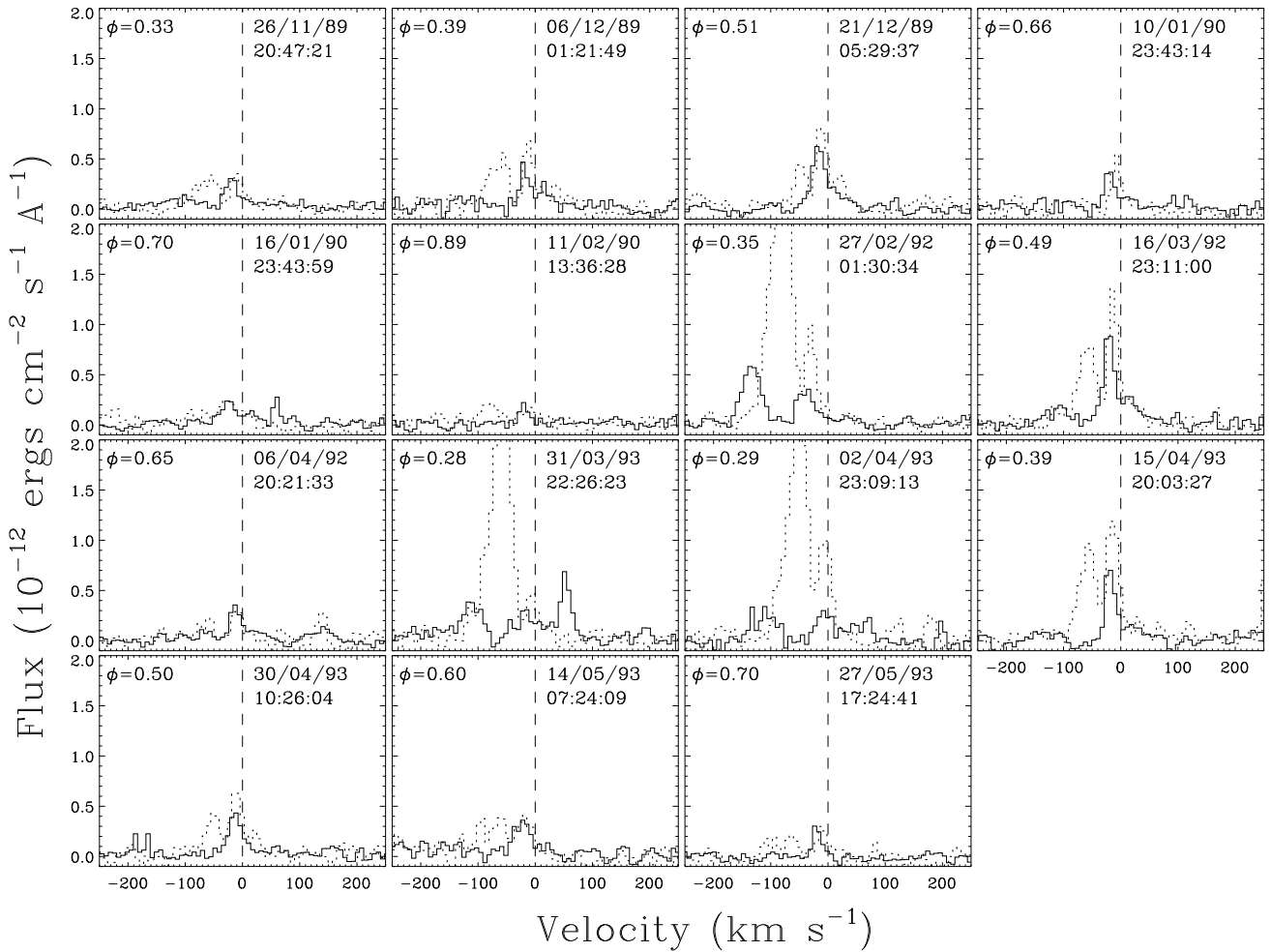


Fig. 7.— Same as Fig. 3, for L² Pup.

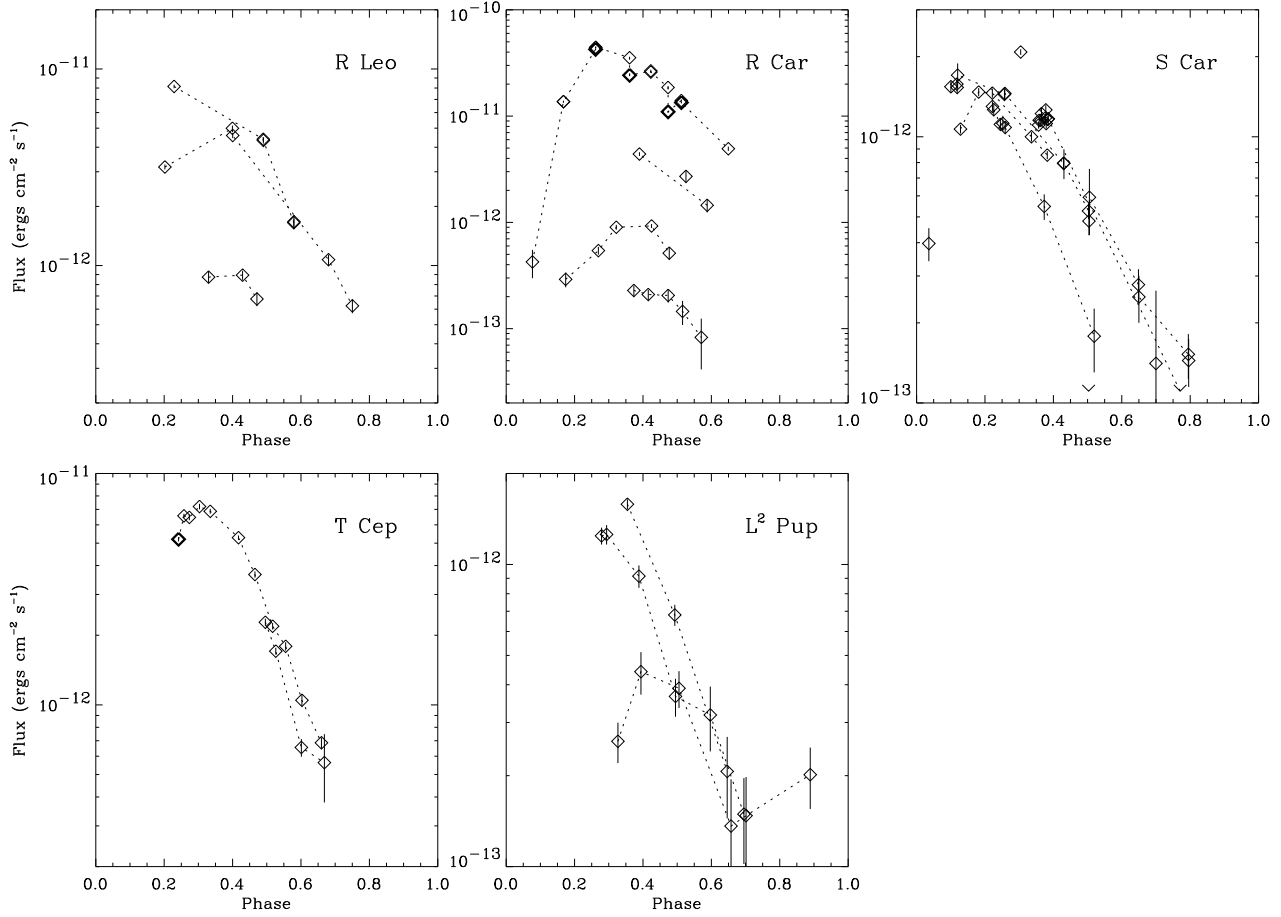


Fig. 8.— The Mg II h line fluxes measured from IUE LW-HI spectra, plotted versus pulsation phase. Dotted lines connect points within the same pulsation cycle. Thick symbols identify potentially inaccurate data points due to overexposure, as indicated by NEWSIPS data quality flags.

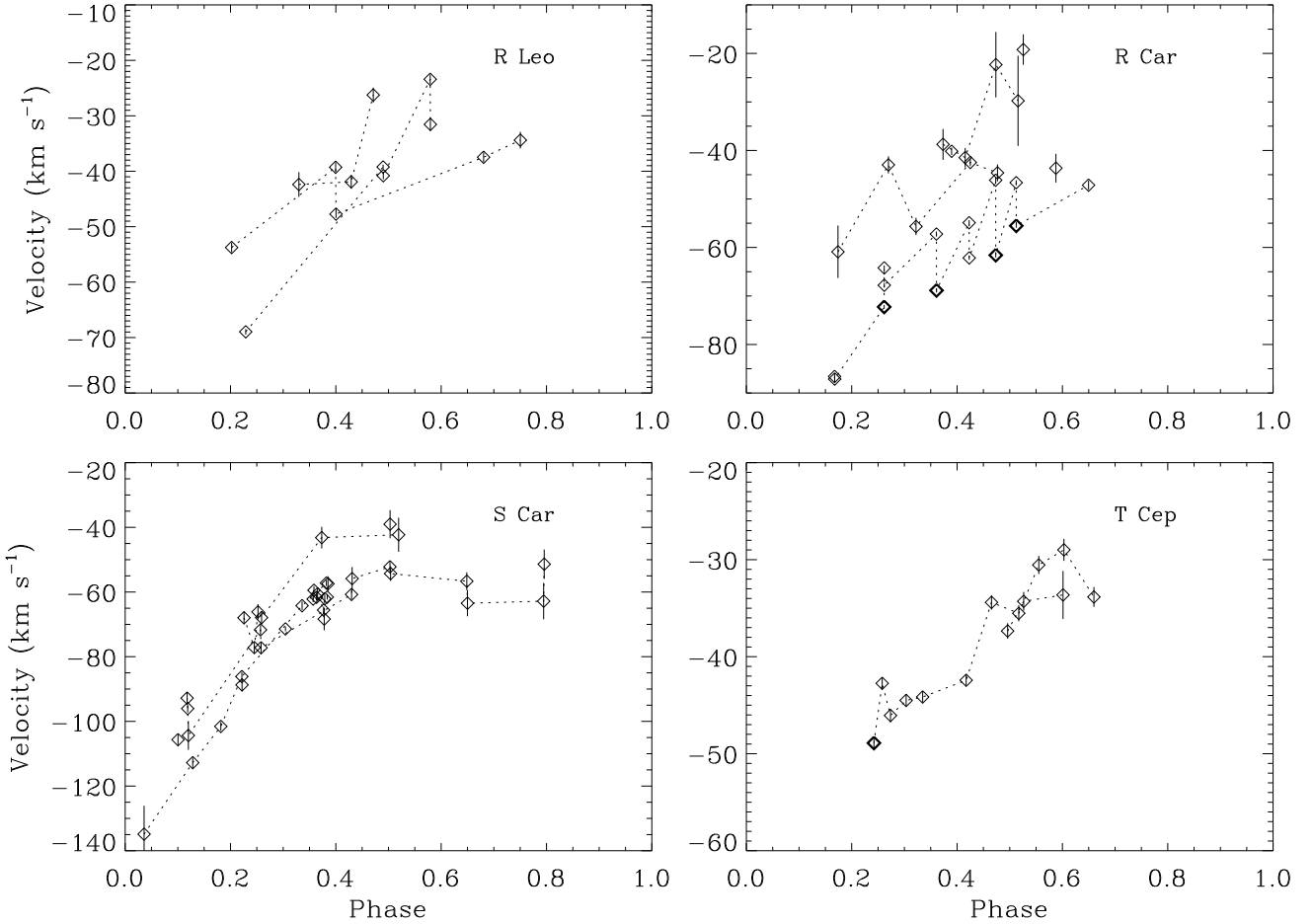


Fig. 9.— The Mg II h line centroid velocities measured from IUE LW-HI spectra in the stellar rest frame, plotted versus pulsation phase. Dotted lines connect points within the same pulsation cycle. Thick symbols identify potentially inaccurate data points due to overexposure, as indicated by NEWSIPS data quality flags.

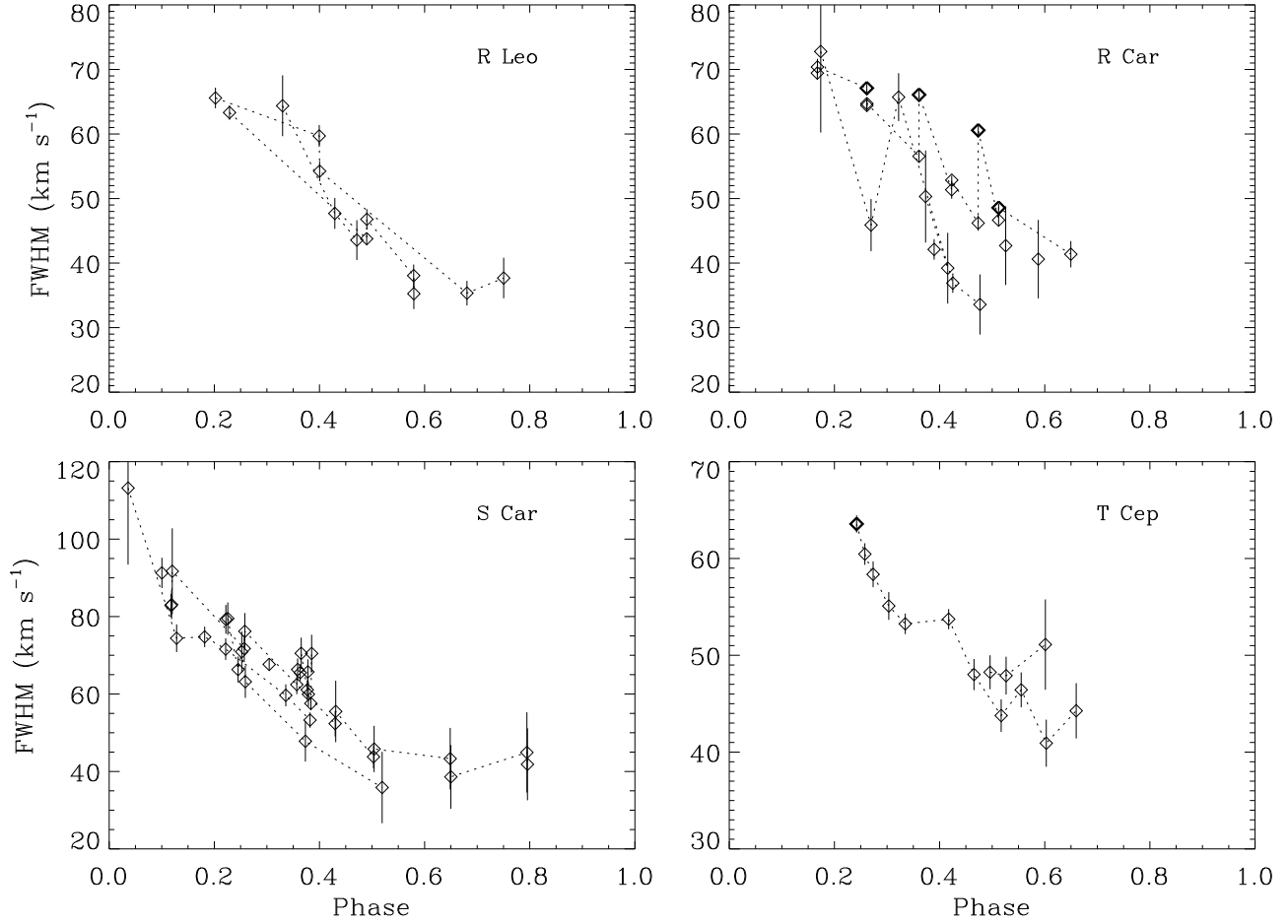


Fig. 10.— The Mg II h line widths measured from IUE LW-HI spectra, plotted versus pulsation phase. Dotted lines connect points within the same pulsation cycle. Thick symbols identify potentially inaccurate data points due to overexposure, as indicated by NEWSIPS data quality flags.

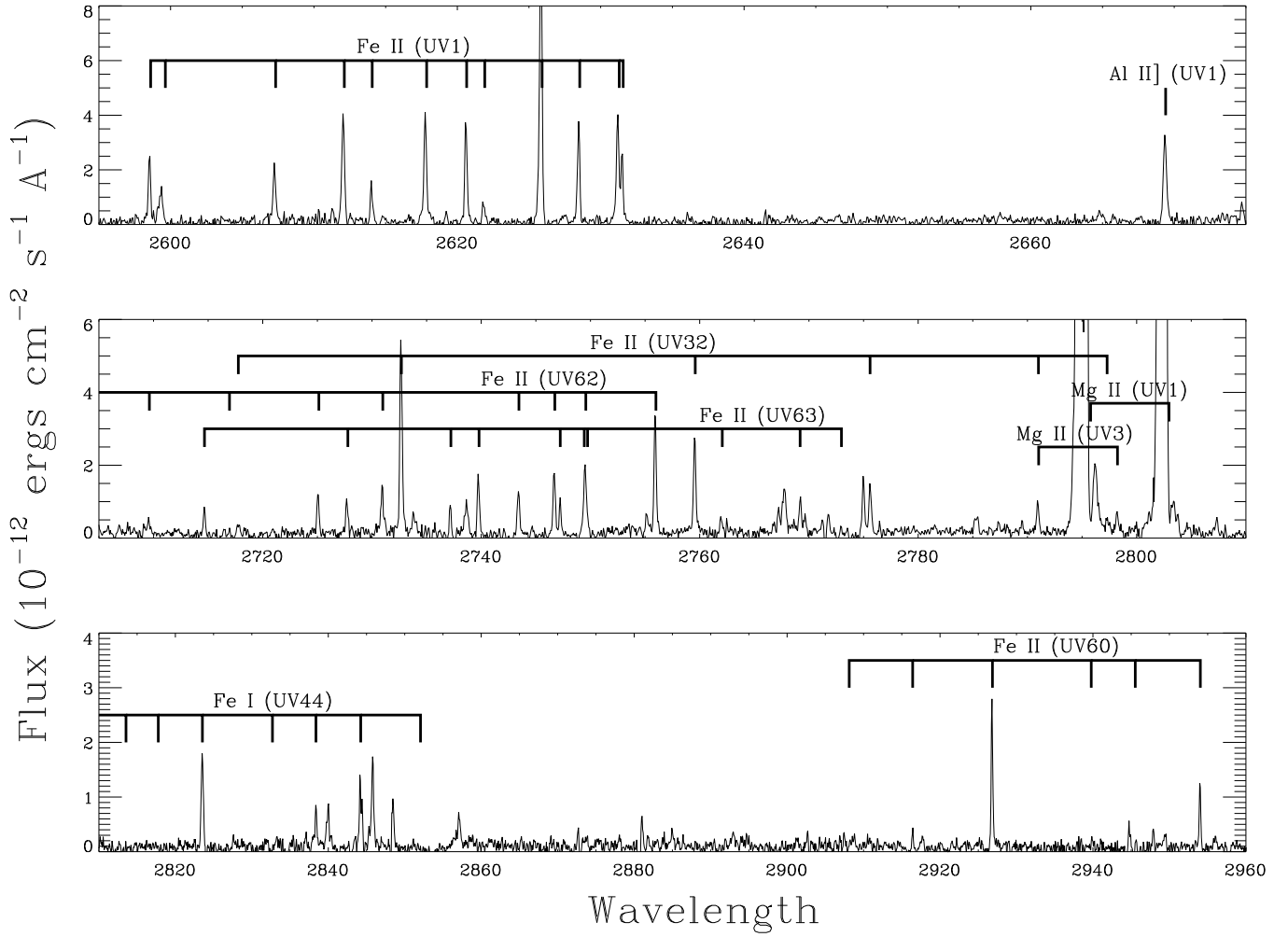


Fig. 11.— Sections of an IUE LW-HI spectrum (LWP17263) of R Car obtained on 1990 January 30. Expected line locations are displayed for several multiplets, which account for most of the lines seen in the spectrum.

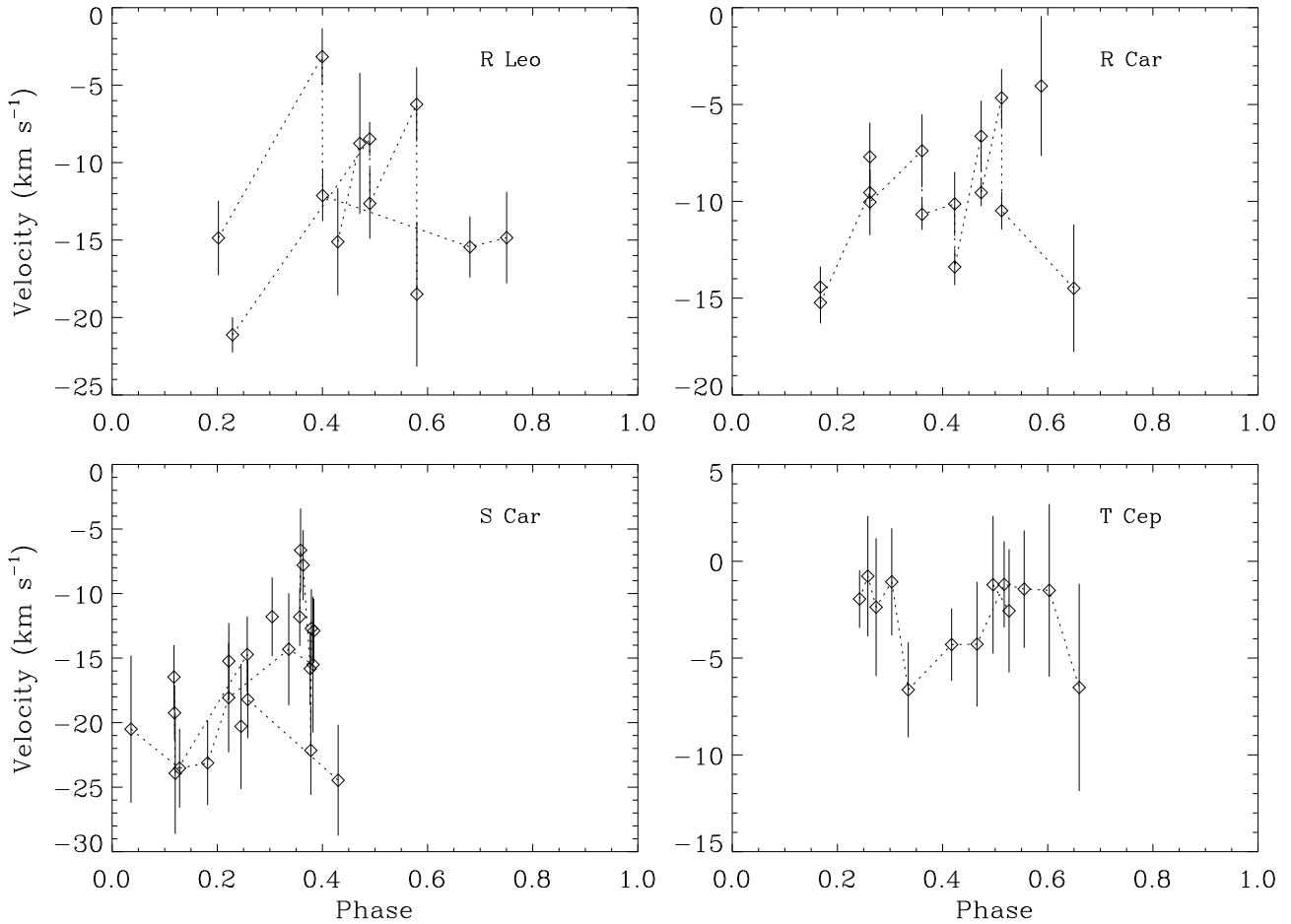


Fig. 12.— The centroid velocities of the Fe II 2625.667 Å line in the stellar rest frame, measured from IUE LW-HI spectra and plotted versus pulsation phase. Dotted lines connect points within the same pulsation cycle.